Exp Fluids
DOI 10.1007/s00348-009-0806-3

RESEARCH ARTICLE

# The use of plasma actuators for bluff body broadband noise control

**Yong Li · Xin Zhang · Xun Huang**

Received: 7 July 2009 / Revised: 20 December 2009 / Accepted: 21 December 2009


**Abstract** Experiments were conducted using plasma actuators to control broadband noise generated by a bluff body flow. The motivation behind the study was to explore the potential of plasma actuators to reduce landing gear noise during approach phase of an aircraft. The control effectiveness of both dielectric barrier discharge and sliding discharge plasma actuators were tested in laboratory environment, using a representative bluff body consisting of a circular cylinder and an oblique strut. Noise measurements were taken in an anechoic chamber using a phased microphone array and far-field microphones. Results showed that the upstream directed plasma forcing, located at ±90 deg on the upstream cylinder with respect to the approaching flow, could effectively attenuate the broadband noise radiated from the wake flow interaction with the downstream strut. With the same AC electrical power consumption, the sliding discharge with additional DC voltage was found to be more effective due to its elongated plasma distribution and higher induced flow momentum. Measurements using particle image velocimetry suggested that the flow speed impinging on the downstream strut was reduced by the upstream plasma forcing, contributing to the reduced noise.

Y. Li (✉) · X. Zhang
Airbus Noise Technology Centre, Department of Aeronautics and Astronautics, University of Southampton, Southampton SO17 1BJ, UK
e-mail: y.li@soton.ac.uk

X. Zhang
e-mail: x.zhang1@soton.ac.uk

X. Huang
Department of Mechanics and Aerospace Engineering, Peking University, Bejing 100871, China
e-mail: huangxun@pku.edu.cn

**List of symbols**

| | |
|---|---|
| $D$ | Cylinder diameter |
| $L$ | Cylinder length |
| $Re_D$ | Reynolds number based on cylinder diameter $D$ |
| $x, y, z$ | Cartesian coordinates |
| $U_\infty$ | Free stream speed |
| $U$ | Streamwise ($x$) velocity |
| $V$ | Normal ($y$) velocity |
| DBD | Dielectric barrier discharge |
| SD | Sliding discharge |
| $V_{p-p}$ | Peak to peak high AC voltage |
| $f$ | Frequency |
| PIV | Particle imaging velocimetry |
| SPL | Sound pressure level |

## 1 Introduction

Over the past few decades, the popularity of air travel has increased significantly, which has led to increase in air traffic and drawn the attention of communities that live near airports to the problem of noise pollution (Raman and McLaughlin 2000). Airframe noise has been widely demonstrated to be a main contributor of aircraft noise during the approach to landing phase, especially when the aircraft is equipped with modern high bypass ratio engines (Crighton 1991; Macaraeg 1998). Since airframe noise is normally caused by the interactions between the aircraft surface geometry and turbulent flow, various flow control strategies, including passive and active control methods (Gad-el 2000), have been explored to modify the flow structures around the airframe components to reduce the corresponding aerodynamically generated noise. A main

Published online: 06 January 2010

source of airframe noise is the landing gears where fairings can be applied, potentially leading to a reduction of radiated noise by shielding the downstream components from the oncoming flow (Dobrzynski et al. 2002; Piet et al. 2005; Molin et al. 2006). This form of passive control is limited by practical considerations such as the need for easy access for maintenance and weight increase.

Plasma technique has been widely demonstrated to be able to modify the local flow by introducing extra momentum (Moreau 2007) and therefore offers a potential to reduce flow-induced noise. Recently, dielectric barrier discharge (DBD) plasma actuators have attracted some attentions in aerospace applications (Post and Corke 2003, 2004, 2005; Corke et al. 2004, 2006; Benard et al. 2007, 2008; Jolibois et al. 2008). A surface DBD plasma actuator (Roth et al. 1998, 2000; Roth 1998) generally consists of two electrodes which are flush mounted on both sides of a dielectric plate. One of the electrodes is exposed to the ambient air, and the other is insulated by a dielectric material. A high AC voltage of a particular waveform (e.g. sine or square waveforms) applied to the exposed electrode weakly ionizes the atmospheric air adjacent to the exposed electrode. The ionized air (plasma) in the presence of the electric field gradient produced by the electrodes results in a body force that acts on the external air to induce airflow along the actuator surface. Some recent works have demonstrated the potential of the DBD plasma actuators on the attenuation of the flow-induced noise. For a cavity driven by a low-speed flow, plasma actuators were found to be able to attenuate flow-induced tonal noise either through manipulating the shear layer or through generating disturbances at an off-resonant frequency (Chan et al. 2007; Huang et al. 2008; Huang and Zhang 2008). For a bluff body, such as circular cylinder, a preliminary study using DBD plasma actuators suggested a potential for broadband noise reduction (Thomas et al. 2008) by reducing the degree of flow separation and eliminating the associated Karman vortex shedding.

DBD plasma actuators are now the most widely used discharge actuators for airflow control (Moreau 2007). Nevertheless, the extent of the luminous plasma area is often limited to several millimetres, which might be a crucial drawback for engineering applications with a model of a sufficient size, especially for commercial air transport on landing approach. On the other hand, a sliding discharge (SD) actuator consisting of AC DBD and additional DC voltage in air has the advantage of producing elongated plasma sheet when compared to DBD plasma, and the discharge is very stable (Tsikrikas and Serafetinides 1996; Louste et al. 2005; Moreau 2007). Moreau et al. (2008) provided some details about the characteristics of SD discharge and its effect on the boundary layer of low-velocity flow.

In this work, the primary objective was to demonstrate the use of plasma actuator technology for landing gear noise control. Both DBD plasma actuators and SD plasma actuators were initially employed to investigate the effectiveness of the plasma in attenuating broadband noise generated by a bluff body. The bluff body consisting of a circular cylinder and an oblique I-shape strut represents an idealized model of the main leg part of a landing gear. The plasma actuators were designed and installed on the surface of the bluff body model to create a plasma distribution that acts as a virtual fairing, which can effectively modify the flow around the bluff body. The performances of these two kinds of plasma actuators on a flat plate were firstly measured by a glass Pitot tube. Aeroacoustic measurements were then undertaken in an open jet tunnel located in an anechoic chamber facility using both a phased microphone array and far-field microphones on the noise control of the bluff body. Particle imaging velocimetry (PIV) measurements were also taken in a low-speed open-loop wind tunnel to provide insight into the physics of flow/noise control mechanism.

## 2 DBD and SD plasma actuators

A schematic of single DBD plasma actuator is given in Fig. 1a. When a sufficient high AC voltage is applied to the electrodes, the discharge ignites at the edge of the exposed electrode (1). A SD plasma actuator consists of three electrodes, combining both a DBD actuator and a DC corona discharge actuator (Moreau et al. 2006, 2008), as shown in Fig. 1b. The lower electrode is connected to a high AC voltage, while the upper two exposed electrodes are connected to a high DC voltage. The direction of the induced wind depends on the polarity of the DC voltage. When the DC voltage supplied to the electrode (1) is negative, the induced wind is from left to right (as shown in the figure), and vice versa. A plasma distribution can be found between the two on-surface electrodes and much more elongated by the SD actuator compared to the DBD actuator. This larger plasma sheet might be advantageous for applications with a large-scale model.

Measurements were taken to determine the induced wind speeds by a single plasma actuator based on DBD and SD. The system consisted of a high voltage AC and DC power supply unit and a high-frequency signal generator (TTiTG550). All the three electrodes are made of copper tape with 0.076 mm thickness, and the dielectric plate is made from silicon rubber of 1 mm thickness. Electrodes (1) and (2) are 10 mm wide, and electrode (3) is 20 mm wide. Although it was reported (Dai and Roth 2005) that the maximum induced velocity occurred when the gaps between the electrodes (1) and (3), electrodes (2) and (3)

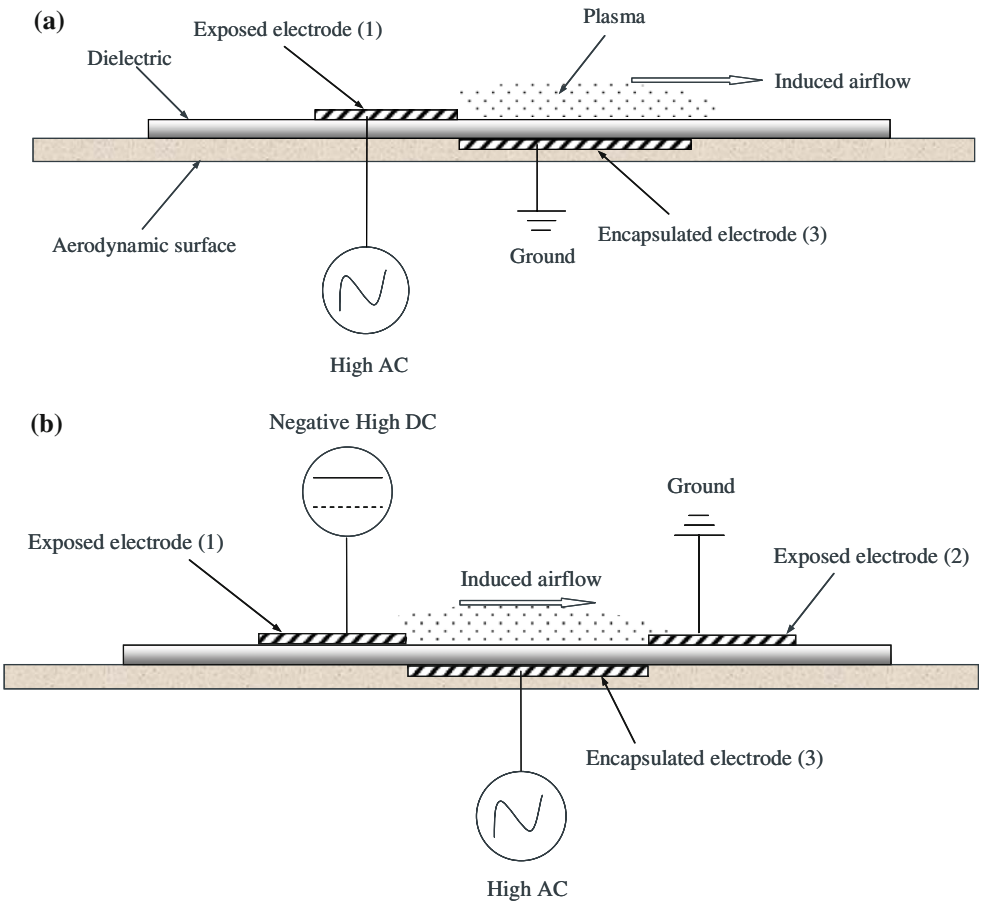


**Fig. 1** Schematic *side view* of the plasma actuators (not to scale). **a** DBD plasma actuator. **b** SD plasma actuator

were between 1.0 and 2.0 mm, the gaps were set to zero. A strip of Kapton tape was used to cover the electrode (3) to prevent inner discharge. The AC high voltage, generated by amplifying a small sine wave signal using an amplifier, was applied to the exposed electrode (1) for the DBD plasma actuator and to the encapsulated electrode (3) for the SD plasma actuator. The high voltage applied to the electrodes and the electric currents were monitored by a digital oscilloscope (Tektronix TDS5034B). The signal was generated using a low-voltage general purpose waveform generator, which enables us to generate an alternating voltage with an arbitrary waveform, such as sine wave, square wave and saw wave. Nevertheless, only the first two waveforms did work for the applied power supply unit. The sinusoidal waveform was then employed in the present study since it was found that there were only little performance differences between the two waveforms on the DBD and the SD plasma actuators.

Some illustrated plasma sheets on the surface of the dielectric plate for the DBD and the SD plasma actuator are shown in Fig. 2. For the DBD plasma actuator, the electrode (2) was left unconnected. The spanwise uniform plasma sheet is only about 6 mm wide and adjacent to the electrode (1). For the SD plasma actuator, the on-surface exposed electrodes (1) and (2) were connected to a high DC voltage and a much wider and luminous plasma sheet is visible over the area between them. The flow velocities induced by the both plasma actuators were measured by a Pitot probe which is made of glass to avoid any electric interference with the plasma. The outer and inner diameters of the tube are 1.0 and 0.61 mm, respectively. The accuracy for the velocity measurement is within $\pm 0.1$ m/s. The measurements were taken at the middle span of the plate, assuming that the velocity profile is uniform along the spanwise direction. The high AC voltage applied on the electrode (1) for the DBD or on the electrode (3) for the SD plasma actuator was a sine wave of $V_{p-p} = 15$ kV at $f = 12$ kHz that provided a reasonable uniform discharge along the spanwise direction. Increasing the input voltage further could produce a higher induced velocity but could also damage the plasma actuator system after the appearance of the filamentary structure. A negative DC voltage of $-12$ kV was supplied to the on-surface electrode (1) for the sliding discharge.

The mean induced velocity profile for the two discharges at 25 mm downstream from the right edge of the

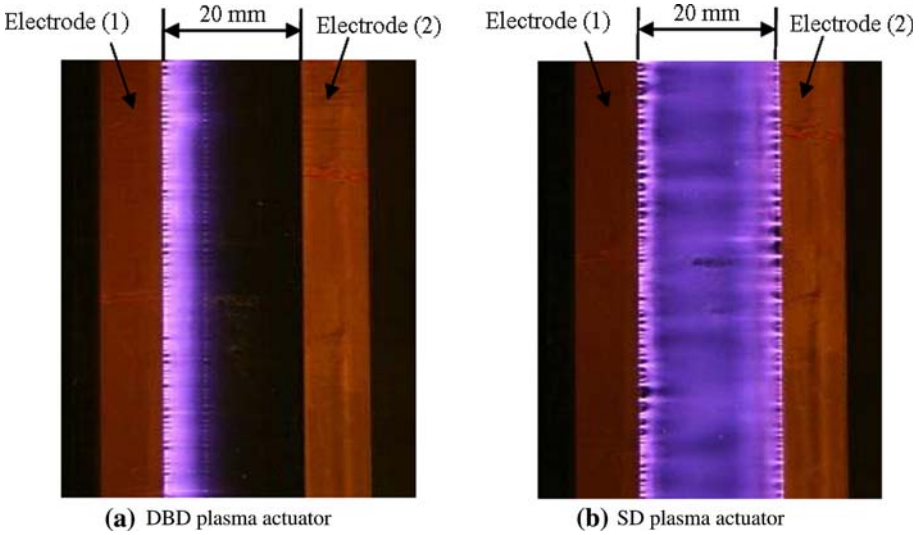


**Fig. 2** Plasma sheets generated by the DBD and SD on the surface of the dielectric plate (induced flow is from *left* to *right*)

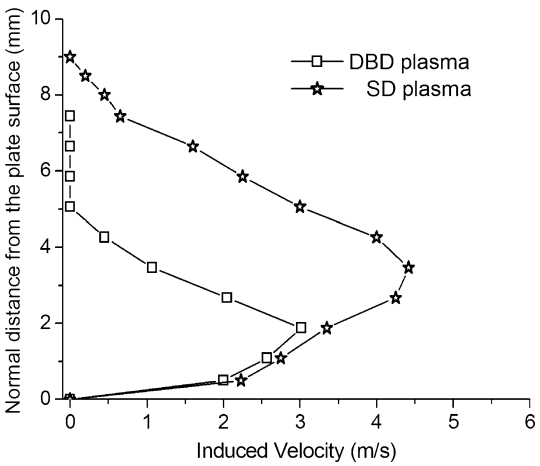


**Fig. 3** Induced airflow speeds by the DBD and SD at 25 mm from the edge of the electrode (1)

electrode (1) is shown in Fig. 3. The velocity profile shows that the height of the induced air flow layer for the DBD plasma actuator was 5 mm, which was about a half of that produced by the SD plasma actuator. At this downstream position, the maximum speed obtained at a normal distance of 2 mm above the surface with the DBD actuator was increased by approximately 50% with the SD actuator. The higher normal position (3.5 mm from the plate surface) of the maximum speed indicates that the induced airflow by the SD separates from the dielectric surface much further than that induced by the DBD. This is due to the counter wind produced at the DC electrode (2) because of high electric field that pushes away the oncoming induced air flow from the surface. Based on the measured velocity profile at this location 25 mm from the edge of the electrode, shown in Fig. 3, and assuming that the induced flow is spanwise uniform, we can summarize through integration of velocity profile that the induced flow momentum by the SD is three times higher than that induced by the DBD. This much higher induced flow momentum might be crucial for large scale application.

## 3 Flow and noise control measurements

### 3.1 Testing model and plasma actuator position

To demonstrate the control capabilities of the plasma in the geometry relevant to a landing gear, two surface-mounted plasma actuators (DBD or SD actuator) were applied on both sides of a bluff body model that consists of a circular cylinder and an oblique I-shape strut, as schematically shown in Fig. 4. The model represents an idealized model of the main leg parts of a landing gear. The cylinder model is ($D$=) 100 mm in diameter and ($L$=) 500 mm in length. The width of the I-shape oblique strut is 70 mm. The plasma actuators with 1 mm thickness silicon rubber as dielectric layer were wrapped on the surface of the cylinder, and the edge of the exposed electrode (1) was located on the cylinder at ±90 deg with respect to the approaching flow. Other locations were also extensively tested but were found to be less efficient for wake flow control. The electrodes span from the top end of the cylinder across the cylinder area that covers the downstream oblique strut. The induced plasma forcing in two directions, i.e. generally upstream directed and downstream directed, was tested in the experiments.

### 3.2 Facilities and test setup

The acoustic control measurements were taken in the Southampton DARP anechoic chamber equipped with an open jet nozzle, as shown in Fig. 5. The open jet consists of

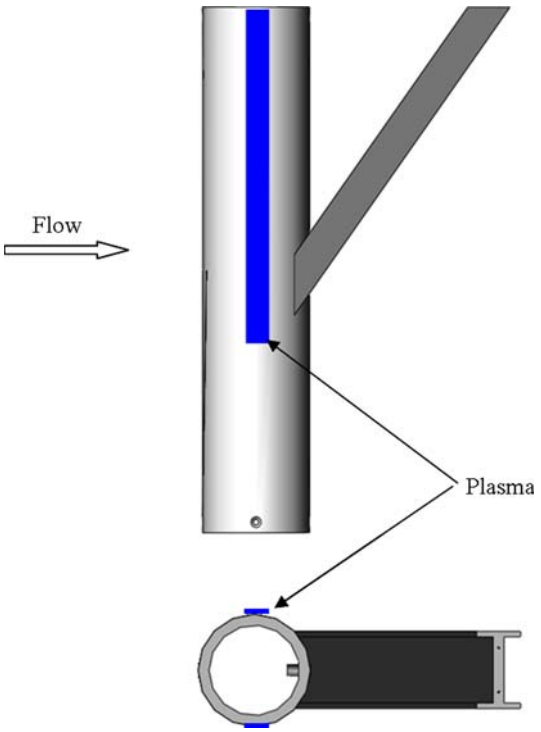


**Fig. 4** Schematic of the testing model and plasma location on the cylinder and oblique I-shape strut (not to scale)

a nozzle connected to a high pressure source through a series of silencers. A 10:1 contraction ratio nozzle with a rectangular exit of 0.35 m × 0.5 m (width by height) was used in the tests. The bluff model was positioned 0.3 m downstream from the nozzle exit and installed between two Perspex end-plates that were flush mounted to the two sides of the nozzle to prevent the wake from spreading in the spanwise direction. The free stream speeds ($U_\infty$) employed in the tests ranged between 20 and 40 m/s, resulting in Reynolds numbers ($Re_D$) between $1.7 \times 10^5$ and $3.4 \times 10^5$ based on the cylinder diameter $D$.

Flow field measurements using PIV were also conducted to investigate the turbulent wake downstream of the cylinder and the flow interaction with/without the plasma actuation. The PIV measurements were taken in an open-loop wind tunnel. The maximum flow speed attainable in the uniform work section (0.9 m × 0.6 m) of the tunnel was 35 m/s. The ceiling and port side of the tunnel test section were fitted with Perspex panels that allowed a camera to view from top and laser light to penetrate from sidewall. Figure 6 shows a schematic of the model setup in the tunnel and the corresponding coordinates. The PIV surveys were performed at two wind tunnel speeds of 20 and 30 m/s to acquire flow field measurements in the plane, $x$–$y$, parallel to the wind tunnel floor and at $z = 0$ mm corresponding to the plane 150 mm above the wind tunnel floor.

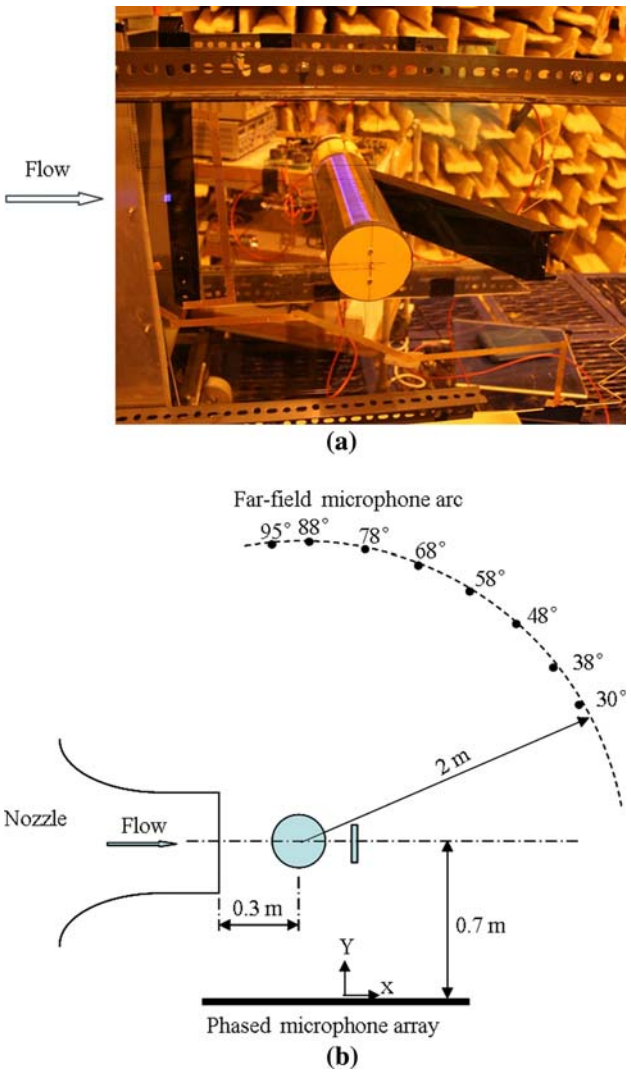


**Fig. 5** Test setup. **a** Near view showing the model between two Perspex end-plates; **b** Schematic of the anechoic chamber noise measurements setup (not to scale)

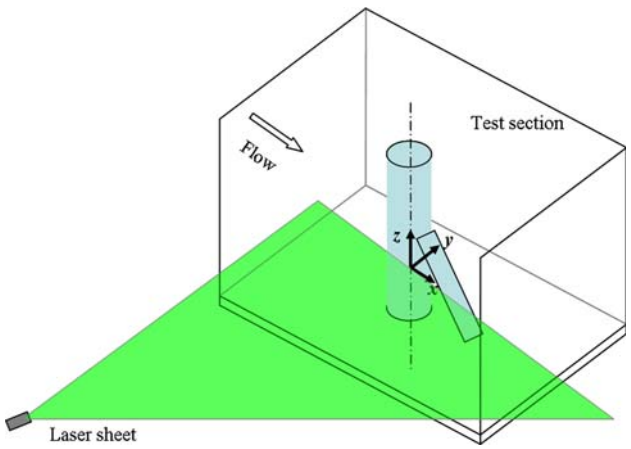


**Fig. 6** Schematic of the cylinder in the tunnel test section and the definition of the coordinates system for PIV tests

### 3.3 Measurement techniques

The noise level was measured using a phased microphone array and far-field microphones in the anechoic chamber, as also shown in Fig. 5. The 0.63-m-diameter phased microphone array consisted of 56 omnidirectional electrets condenser microphones with a frequency response range of 20–20 kHz. These microphones were calibrated using a reference ½′ B&K microphone that was located adjacent to each microphone and a point source of white noise on the wind tunnel floor. This microphone array was used to localize the noise sources on the model using beamforming technique (Dougherty 2002). The scan plane (which crosses the centre line of the cylinder and strut) was 0.7 m to the surface of the microphone array. The origin for the scan plane was located on the centre of the microphone array. The far-field microphone array consisted of 8 microphones which were installed on an arc that was approximately 2 m away from the model. The elevation angle of each microphone was 95, 88, 78, 68, 58, 48, 38 and 30 degs, respectively. All the 8 microphones were covered by wind shields to alleviate the wind effects on the acoustic measurements. The microphones have a good linear frequency response, and an omnidirectional polar pattern that help to ensure the quality of the measurements.

All the phased microphones and far-field microphones were connected to the National Instruments PXI-4472 modules via pre-amplifiers. The data were sampled at 48 kHz and were analysed using a block size of 4,096, yielding a frequency resolution of about 12 Hz. To reduce spectral leakage, a Hanning window function was applied to each single block before performing fast Fourier analysis and a total of 100 blocks were averaged for statistic confidence.

The PIV system employed in the open-loop wind tunnel tests was a Dantec dynamics system with a New Wave Gemini Nd:YAG dual laser. A Dantec HiSense 1,024 × 1,289 resolution CCD camera was set up perpendicular to the laser sheet on the scan plane and fixed on a support structure installed on the ceiling of the work section. A total of 200 images of the flow field were taken for each experimental condition. Each image set was processed using a 32 pixel × 32 pixel cross-correlation area and a 50 × 50% overlap to improve the resolution of the vector map. The spurious vectors on the map were then further removed using a range validation, whereby vectors greater than a specified magnitude would be rejected. The shadow area was removed before processing by making marks on the image map because this area produces bad vectors due to no laser in that area.

Due to the resolution of the camera, the envisaged area of the flow structures was limited to one half of the cylinder wake and the camera looked down from the ceiling. Only the sliding discharge was applied in this section of flow visualization, and the power supply and the plasma configuration were kept at the same levels as the ones used in the anechoic chamber tests.

## 4 Experimental results

This section summarizes a series of flow-noise control experiments using two plasma actuators located on the upstream located circular cylinder as previously described. The effects of the plasma actuators on the flow at different plasma forcing directions were performed for three free stream speeds of 20, 30 and 40 m/s (corresponding Reynolds numbers $Re_D$ between $1.7 \times 10^5$ and $3.4 \times 10^5$ based on the cylinder diameter $D$).

### 4.1 Aeroacoustic measurements

The noise source distribution with and without the upstream directed plasma forcing was firstly measured using the phased microphone array. Figure 7 shows the noise source maps at two frequencies of 2 and 4 kHz measured at a free stream velocity of 30 m/s from left to right. A conventional beamforming technique (Dougherty 2002) was used to process the microphone array data. The upstream directed plasma forcing applied here was generated from the sliding discharge plasma actuator. The gap between the exposed electrodes (1) and (2) was 20 mm, and a −12 kV DC voltage difference was applied on between them. The high AC voltage with sine wave of about 15 kV at 12 kHz was connected to the insulated electrode (3) separated from the exposed electrodes. Under the current condition, the actuator generated a steady and bright plasma sheet on the surface. The two horizontal lines in the figure represent the two end-plates, which shows that only part of the cylinder (about 350 mm in length) and the whole oblique strut are installed between them. The comparison between the two plots with and without the upstream directed plasma shows that the major noise sources at these two frequencies located in the gap area between the cylinder and the strut, and the noise level was reduced by a considerable amount when the plasma was activated. For the lower frequencies less than 1 kHz, this microphone array failed to localize the noise sources due to the poor spatial resolution in low-frequency region.

Measurements using the far-field microphones also suggest significant noise attenuation within a broadband frequency range for all the test speeds except 40 m/s, as shown in Fig. 8. The plots shown are the sound pressure level (SPL) differences between plasma on and off conditions, obtained in 1/3-octave band spectra. The data were recorded by averaging the results from all the far-field microphones, and therefore it gave the mean noise

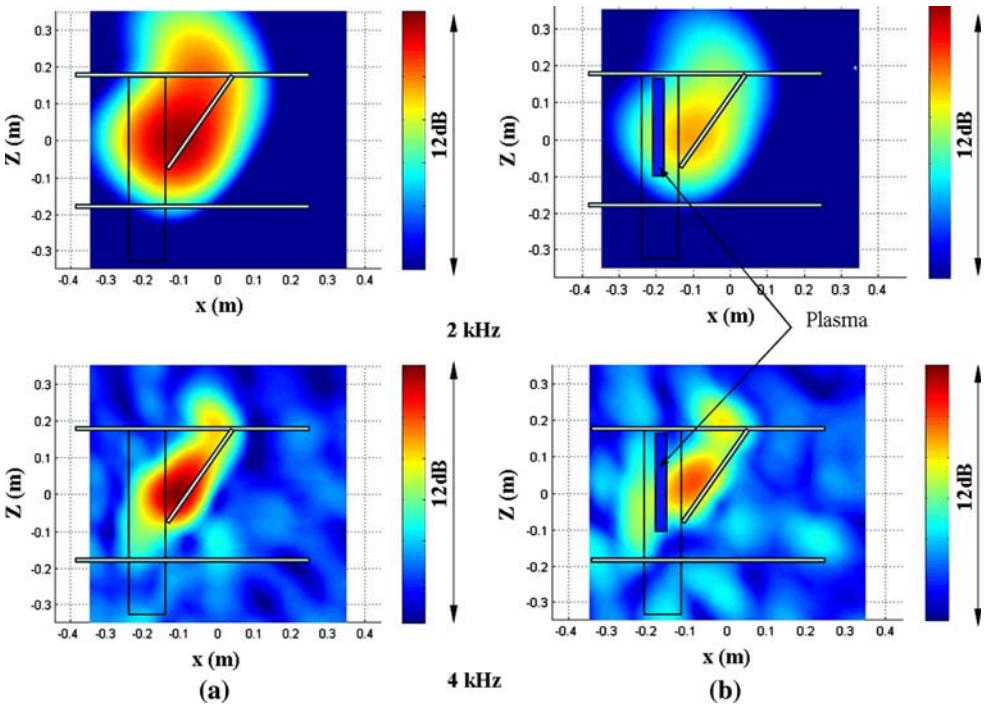


**Fig. 7** Noise source maps at 2 and 4 kHz from the phased microphone array test. **a** Plasma off; **b** Plasma on. Free stream speed of ($U_\infty$=) 30 m/s is from *left* to *right* and plasma control is from the upstream SD)

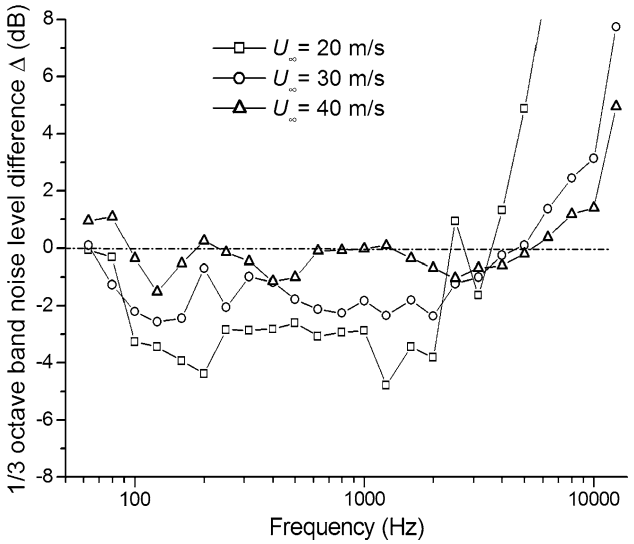


**Fig. 8** Broadband noise reduction by averaging the data from all the far-field microphones. Results are from upstream sliding discharge

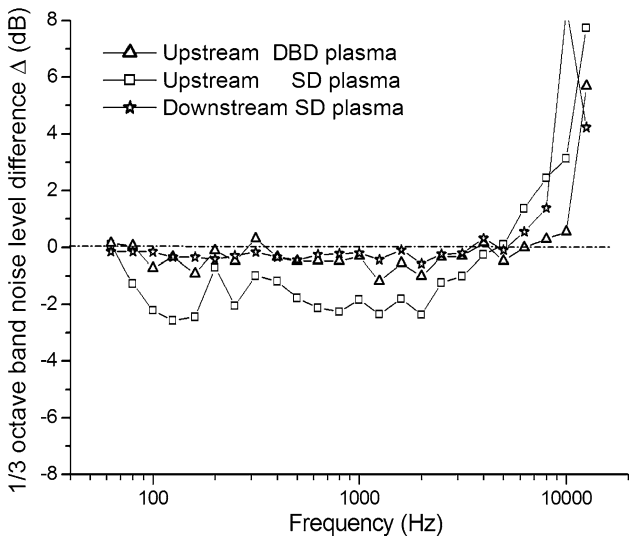


**Fig. 9** Comparison of noise attenuation between the DBD and the SD plasma actuators at the free stream speed of 30 m/s

reduction at the far positions. Reductions of −3.8 dB and −2.2 dB were obtained in the frequency ranging between 80 and 4 kHz at free stream speeds of 20 and 30 m/s, respectively. The slightly noise level increase at around 3 kHz at the speed of 20 m/s was due to the tonal noise radiated from the jet nozzle, which could be confirmed by the beamforming technique. This tonal noise contaminated the broadband noise from the bluff body, especially at lower wind speeds. The large noise increases at high frequencies above 6 kHz were due to the dominating self-noise of the sliding discharge plasma actuator. It can be seen that with increasing the free stream speed the current plasma actuator under this fixed authority gradually lost its effectiveness in noise control.

A comparison of noise reduction between the upstream directed DBD plasma forcing and the upstream directed SD plasma forcing is shown in Fig. 9. It shows that the SD is more effective than the DBD at the frequencies below 6 kHz, mainly due to the elongated plasma distribution and a higher induced flow momentum as described in Sect. 2. The disadvantage of the SD is that it increases more plasma self-noise level at the frequencies above 6 kHz than the

DBD plasma actuator. The comparison of the downstream directed SD plasma forcing (in the same direction as the external flow) is also shown in Fig. 9. The downstream directed plasma is not as effective as the upstream directed one on the control of bluff body broadband interaction noise. Although the downstream forcing at this location was reported to reduce the cylinder wake width and suppress the vortex shedding from a single cylinder (Thomas et al. 2008), the downstream plasma forcing on the cylinder in this study had little effect on the external flow impinging on the downstream located strut, which will be shown later.

### 4.2 Flow field measurements

To investigate the physics of the observed noise attenuation by the upstream directed plasma actuator, the near wake flow of the cylinder was examined using PIV measurements. Figure 10 shows the time-averaged streamwise U-velocity contours downstream of the cylinder. The effects of (a) upstream directed and (c) downstream directed plasma forcing were compared to the original mean velocity (b) without plasma forcing. The beginning of the envisaged area was about 20 mm downstream from the plasma actuator in order to exclude the bright lights of plasma itself. The local mean flow velocities close to the cylinder were greater than the free stream speed of 20 m/s due to the displacement effect in the cylinder boundary layer. With the upstream directed plasma activated the corresponding maximum velocity close to the cylinder was reduced about 2 m/s when compared to the case without plasma, while the local velocity was increased at the same amount with the downstream directed plasma. The flow field area underneath the oblique I-shape strut could not be displayed. The measurements also showed that the flow shear layer after the cylinder impinged on the downstream strut. The broadband noise radiation was presumably caused by this impingement. With the (a) upstream directed plasma forcing, the width of the wake was increased when compared to the flow (b) without plasma, while impact was not visible when the downstream directed plasma forcing was activated.

To quantify the differences in the downstream wake, the streamwise $U$-velocity profiles are obtained at four $x$ positions ($x = 25$, 50, 75 and 100 mm) downstream from the cylinder centre using the PIV data. The results are shown in Fig. 11. At normal $y$ positions above $-35$ mm for all the four streamwise locations, no data were shown due to the existence of I-beam strut, which prevents the area underneath from viewing by the PIV camera. At the location close to the plasma actuators ($x = 25$ mm), the local streamwise velocity was significantly increased with the downstream directed plasma forcing. At far downstream positions, little difference was observed in the streamwise velocity with the downstream directed plasma, indicating that the downstream plasma forcing worked effectively only on the flow field close to the plasma actuators. The upstream directed plasma increased the cylinder wake width and reduced the streamwise flow speeds at the locations far downstream of the cylinder. As shown in Fig. 10, at this $x$–$y$ plane, the flow impingement on the downstream located I-shape strut would occur at the position of $x = 100$ mm and $y = -40$ mm. At this position (100, $-40$, 0), the streamwise velocity with the upstream directed plasma forcing was about 5 m/s lower than the corresponding velocity without plasma. This reduction in the velocity lessened the impingement, hence attenuating the aerodynamic interaction noise between the cylinder wake flow and the downstream strut. This virtual plasma fairing had the similar effect as the passive control fairing used to reduce the landing gear noise (Dobrzynski et al. 2002; Li et al. 2007; Boorsma et al. 2009) by lessening the flow speed impinging on the downstream components. This result agreed with the findings from the anechoic chamber tests where the upstream directed plasma significantly reduced the noise level at a wind speed of 20 m/s. At 30 m/s, however, the effectiveness of plasma at same input power consumption was reduced.

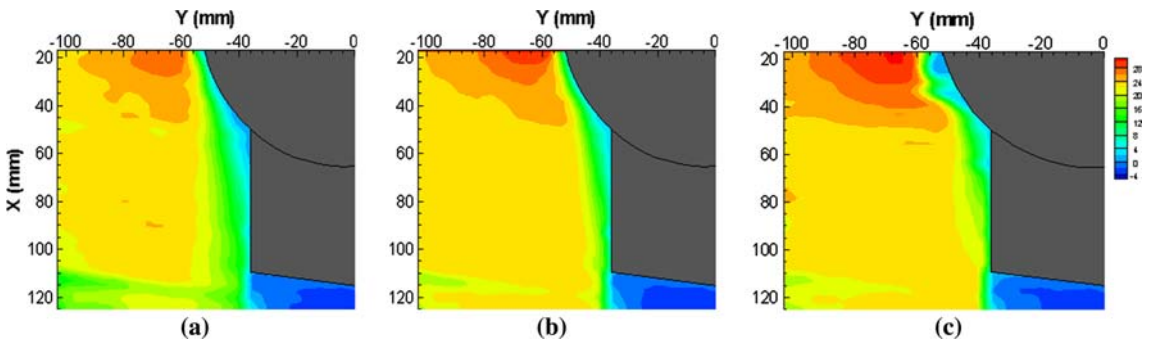


**Fig. 10** Contour plots of time-averaged streamwise $U$-velocity (m/s) in the wake of wind free stream speed of 20 m/s. **a** with upstream plasma forcing; **b** without plasma forcing; **c** with downstream plasma forcing. Flow was from *top* to *bottom*

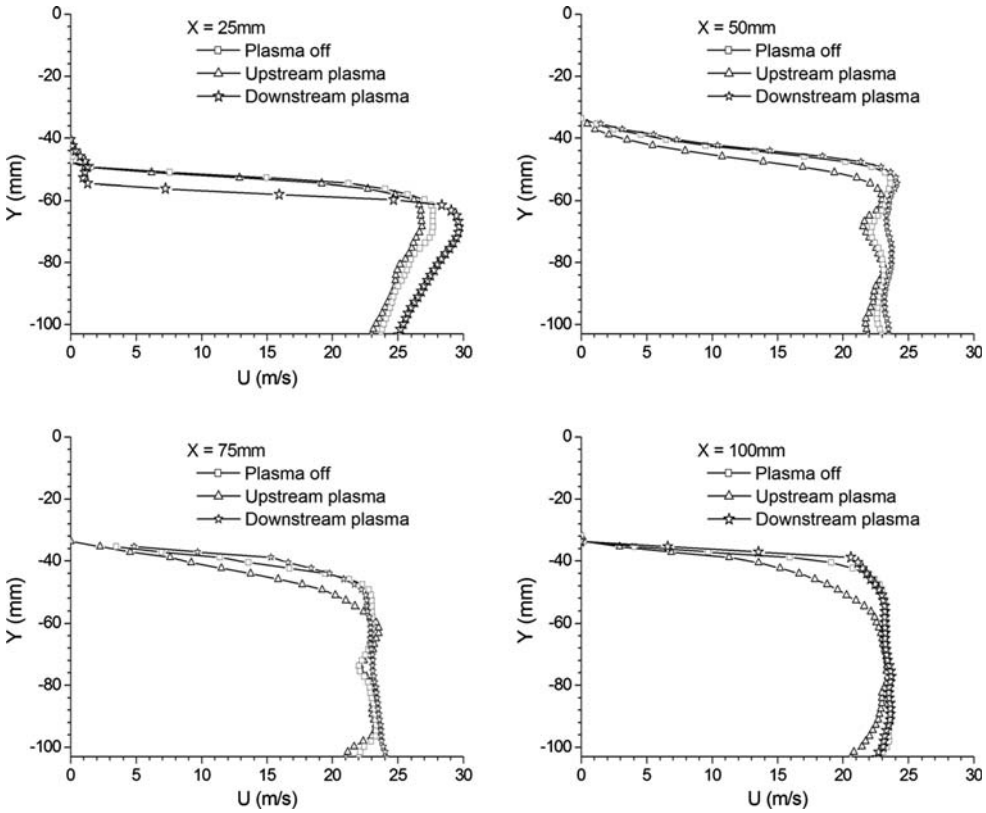


**Fig. 11** Comparison of the streamwise $U$-velocity profiles at 4 different $x$ positions (25 mm, 50 mm, 75 mm and 100 mm) downstream of the cylinder centre

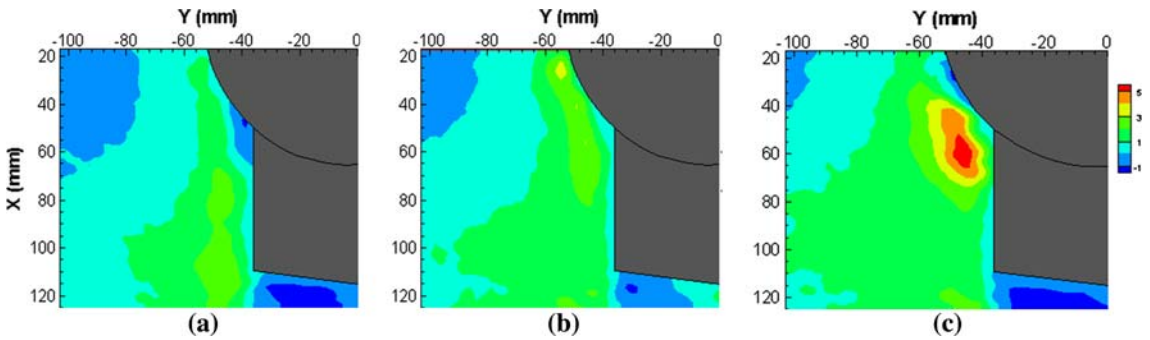


**Fig. 12** Contour plots of time-averaged normal $V$-velocity (m/s) in the wake of wind speed of 20 m/s. **a** with upstream plasma forcing; **b** without plasma forcing; **c** with downstream plasma forcing. Flow was from top to bottom

The normal mean $V$-velocity and the spanwise mean vorticity field for the operation of plasma actuators are shown in Figs. 12 and 13, respectively. The positive increase in the normal direction with the downstream directed plasma forcing suggests that the flow attached further along the surface of the cylinder compared to the cylinder without the plasma. The upstream directed plasma forcing had little effect on the normal velocity. In Fig. 13, the spanwise vorticity field shows that the shear layer contains two centralized vorticity areas that were located in the separation region of the cylinder boundary layer and the impingement region on the oblique strut, respectively. With the upstream direct plasma forcing, the strength of spanwise vorticity in the impingement region was attenuated. However, the downstream direct forcing slightly reinforced the vorticity strength.

Previous studies using plasma actuators for a single cylinder flow and noise control (Thomas et al. 2008) were performed at Reynolds numbers of approximately $Re_D = 3.3 \times 10^4$ based on the cylinder diameter. It was reported that the downstream directed plasma could delay flow separation, eliminate the associated Karman vortex shedding and therefore reduce the vortex shedding-related aerodynamic tonal noise. However, for the broadband interaction noise, the present study demonstrates that plasma actuators are capable of manipulating the turbulent

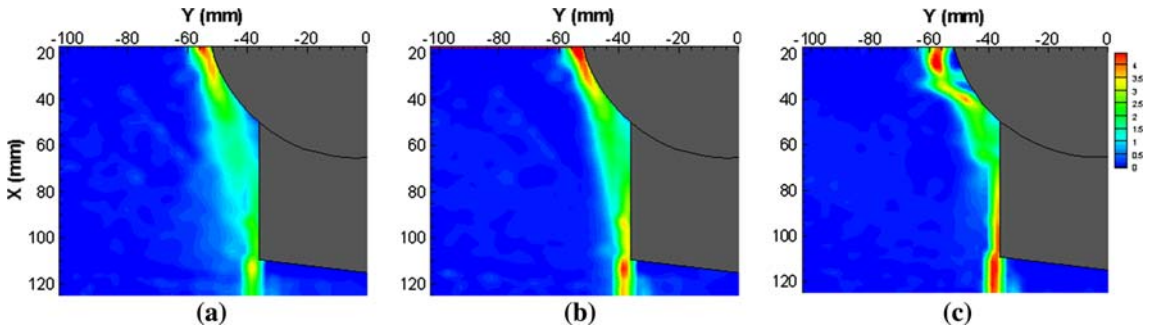


**Fig. 13** Contour plots of time-averaged spanwise vorticity ($msec^{-1}$) in the wake of wind speed of 20 m/s. **a** with upstream plasma forcing; **b** without plasma forcing; **c** with downstream plasma forcing. Flow was from top to bottom

wake of cylinder at a higher Reynolds number of $2.4 \times 10^5$ and with the upstream directed plasma forcing, it can reduce the broadband noise sources generated from the interaction between the cylinder wake and the downstream strut.

## 5 Discussions and conclusions

An experimental study was conducted to explore the potential of plasma actuators to attenuate broadband bluff body noise. Both aeroacoustic and aerodynamic measurements were taken on a representative bluff body consisting of a circular cylinder and an oblique strut, in an open jet located in an anechoic chamber and a low speed open-loop wind tunnel. Microphone array measurements confirm that the major noise sources for this configuration were located in the gap area between the cylinder and the downstream strut. The results demonstrated that plasma actuators could reduce the broadband noise generated by the bluff body. Particularly, it was shown that the upstream directed plasma forcing located on the cylinder surface at $\pm 90$ deg with respect to the approaching flow could effectively attenuate the major broadband noise radiated from the gap area. At the same AC electrical power consumption level, the sliding discharge with additional high DC voltage input is more effective due to its elongated plasma distribution and a higher induced flow momentum when compared to the dielectric barrier discharge. Particle image velocimetry measurements confirm that the noise attenuation with the upstream directed plasma forcing was due to a reduction of the flow speed impinging on the downstream strut. The downstream directed plasma forcing was found to have little effect on the current bluff body configuration in noise control.

The broadband noise radiation by the bluff body could be significantly reduced at the free stream speeds up to 30 m/s under the present actuator authority of sliding discharge. As the wind speed was increased above 30 m/s, the current design gradually lost its effectiveness for flow and noise control. Therefore, for a practical application in the flight of much higher speeds (typical approach speed of about 80 m/s) and Reynolds number, the plasma actuation authority must undergo a commensurate increase. The actuation strategy applied in our experiments presented here is far from optimum since only steady actuation and limited actuators were used. Under the current actuator design, only a little bit higher induced wind speeds could be achieved by increasing the AC and DC voltages before a filamentary structure or sparks between the two surface electrodes appeared, after then the induced speeds dropped dramatically. The shape of the two exposed electrodes for sliding discharge could be optimized to achieve higher DC corona discharge on the surface. The silicon rubber was selected as the dielectric layer for the actuator mainly due to its flexibility to wrap the bluff body, and therefore other materials with improvement in dielectric strength and constant would no doubt improve the actuator performance. Although the $\pm 90$ deg location with respect to the approaching flow is more effective than other locations, there is no doubt that with more actuators distributed on the surface of the bluff body, not just at $\pm 90$ deg, would also achieve higher plasma forcing. This benefit with more actuators has been demonstrated in Thomas et al. (2008).

The significant effect of the concept using direct-upstream plasma forcing presented here demonstrated that the plasma actuator can generate a virtual fairing that partly shields the downstream small component from the oncoming free stream flow, hence reducing the corresponding high-frequency noise. In this case, the plasma works in the same way as the passive control using solid fairings.

**Acknowledgments** The experiments were made possible through the support provided by Airbus Technology Programme CADWIE project monitored by Dr. L. C. Chow, which is gratefully acknowledged.

## References


Benard N, Jolibois J, Forte M, Touchard G, Moreau E (2007) Control of an axisymmetric subsonic air jet by plasma actuator. Exp Fluids 43:603–616

Benard N, Braud P, Jolibois J, Moreau E (2008) Airflow reattachement along a NACA0015 airfoil by a surface dielectric barrier discharge actuator: time-resolved particle image velocimetry investigation. AIAA-2008-4202

Boorsma K, Zhang X, Molin N, Chow LC (2009) Bluff body noise control using perforated fairings. AIAA J 47(1):33–43

Chan S, Zhang X, Gabriel S (2007) The attenuation of cavity tones using plasma actuators. AIAA J 45(7):1525–1538

Corke TC, He C, Patel MP (2004) Plasma flaps and slats: an application of weakly-ionized plasma actuators. AIAA-2004-2127

Corke TC, Mertz B, Patel MP (2006) Plasma flow control optimized airfoil. AIAA-2006-1208

Crighton DG (1991) Aeroacoustics of flight vehicles: theory and practice. NASA RP 1258, chapter: airframe noise 1: 391–447

Dai X, Roth JR (2005) Optimization of a single plasma actuator using the one atmosphere uniform glow discharge plasma. IEEE international conference on plasma science, no. 10525

Dobrzynski W, Chow LC, Guion P, Schiells D (2002) Research into landing gear airframe noise reduction. AIAA-2002-2409

Dougherty RP (2002) Beamforming in acoustic testing. In: Mueller TJ (ed) Aeroacoustic measurements. Springer, Berlin

Gad-el HM (2000) Flow control: passive active and reactive flow management. Cambridge University Press, UK

Huang X, Zhang X (2008) Streamwise and spanwise plasma actuators for flow-induced cavity noise control. Phys Fluids 20(3):037101-1-037101-10

Huang X, Chan S, Zhang X (2008) Variable structure model for flow-induced tonal noise control with plasma actuators. AIAA J 46(1):241–250

Jolibois J, Forte M, Moreau E (2008) Application of an AC barrier discharge actuator to control airflow separation above a NACA0015 airfoil: optimization of the actuation location along the chord. J Electrostat 66:496–503

Li Y, Smith MG, Zhang X, Molin N (2007) Noise sources control of an aircraft landing gear, AIAA-2007-3465

Louste C, Artana G, Moreau E, Touchard G (2005) Sliding discharge in air at atmospheric pressure: electrical behaviour. J Electrostat 63:615–620

Macaraeg MG (1998) Fundamental investigations of airframe noise. AIAA-98-2224

Molin N, Piet JF, Chow LC, Smith M, Dobrzynski W, Seror C (2006) Prediction of low noise aircraft landing gears and comparisons with test results. AIAA-2006-2623

Moreau E (2007) Airflow control by non-thermal plasma actuators. J Phys D Appl Phys 40:605–636

Moreau E, Leger L, Touchard G (2006) Effect of a DC surface-corona discharge on a flat plate boundary layer for air flow velocity up to 25 m/s. J Electrostat 64:215–225

Moreau E, Louste C, Touchard G (2008) Electric wind induced by sliding discharge in air at atmospheric pressure. J Electrostat 66:107–114

Piet JF, Davy R, Elias G, Siller H, Chow LC, Seror C, Laporte F (2005) Flight test investigation of add-on treatments to reduce aircraft airframe noise. AIAA-2005-3007

Post ML, Corke TC (2003) Separation control on high angle of attack airfoil using plasma actuators. AIAA-2003-1024

Post ML, Corke TC (2004) Separation control using plasma actuators-dynamic stall control on an oscillating airfoil. AIAA-2004-2517

Post ML, Corke TC (2005) Overview of plasma glow control: concepts, optimization and applications. AIAA-2005-0563

Raman G, McLaughlin DK (2000) Recent aeroacoustics research in the United States. Noise Vib Worldw 31(10):15–20

Roth JR (1998) Electrohydrodynamically induced airflow in a one atmosphere uniform glow discharge surface plasma. IEEE international conference on plasma science, Institute of Electrical and Electronics Engineers, NJ

Roth JR, Sherman DM, Wilkinson SP (1998) Boundary layer flow control with a one atmosphere uniform glow discharge surface plasma. AIAA-98-0328

Roth JR, Sherman DM, Wilkinson SP (2000) Electro-hydrodynamic flow control with a glow-discharge surface plasma. AIAA J 38(7):1166–1172

Thomas FO, Kozlov A, Corke TC (2008) Plasma actuators for cylinder flow control and noise reduction. AIAA J 46(8):1921–1931

Tsikrikas GN, Serafetinides AA (1996) The effect of voltage pulse polarity on the performance of a sliding discharge pumped HF laser. J Phys D 29:2806–2810